Megapixel digital PCR

Kevin A Heyries[1,2], Carolina Tropini[1,2,6], Michael VanInsberghe[1,2], Callum Doolin[1,2], Oleh I Petriv[1,2], Anupam Singhal[1–4], Kaston Leung[1,2,5], Curtis B Hughesman[3,4] & Carl L Hansen[1,2]

We present a microfluidic 'megapixel' digital PCR device that uses surface tension–based sample partitioning and dehydration control to enable high-fidelity single DNA molecule amplification in 1,000,000 reactors of picoliter volume with densities up to 440,000 reactors cm^{-2}. This device achieves a dynamic range of 10^7, single-nucleotide-variant detection below one copy per 100,000 wild-type sequences and the discrimination of a 1% difference in chromosome copy number.

Advances in basic research and molecular medicine are coupled to the development of ever more precise and sensitive measurement technologies. Quantitative (q)PCR is poorly suited to measurements of absolute concentration, has limited precision (~20%) and presents difficulties in reliably detecting low-copy-number templates owing to nonspecific amplification and competitive side reactions. qPCR measurements are thus sometimes inadequate for applications such as early detection of cancer and monitoring of residual disease[1], analysis of single-cell gene expression[2], and the diagnosis of fetal genetic disorders using small allelic imbalances in circulating DNA[3]. A promising alternative is digital PCR[4], a single-molecule counting technique. Digital PCR works by partitioning a sample at limiting dilution followed by PCR amplification and endpoint detection to identify the presence or absence of template molecules in each reaction. All performance metrics of digital PCR, including sensitivity, precision and dynamic range, improve with the total number of digital reactions. Reduced reaction volumes lead to higher single-molecule detection efficiency, reduced contamination, increased throughput and reduced cost and are thus critical to the development of next-generation digital PCR.

Existing technologies for scalable digital PCR analysis use either microemulsions[5–7] or microfluidics[2,8,9] to implement many small-volume reactions. Although emulsion-based methods have achieved the highest numbers of total reactions, previously developed emulsion-based systems either have poor amplification efficiency[6] or require a complicated workflow[7]. The best-established chip-based implementation of digital PCR, using integrated microvalves, offers advantages of simplified workflow and increased analysis speed. It provides the highest number and density of chambers available in a commercial device (36,960 chambers, ~6,000 chambers cm^{-2}), but scalability is limited by the maximum density at which valves may be reliably fabricated[10].

Here we present a valve-free microfluidic digital PCR device that performs a million single-molecule PCRs in uniform arrays of picoliter-volume chambers with densities up to 440,000 reactions cm^{-2} (Online Methods, **Fig. 1a**,**b** and **Supplementary Fig. 1**).

The sample to be analyzed is first mixed with PCR reagents and injected into a poly(dimethylsiloxane) (PDMS) device containing a bifurcating channel network, with a cross-section of 3 μm × 3 μm, that connects to linear arrays of 10-pl (20 μm × 20 μm × 25 μm) 'dead-end' chambers. The high gas permeability of PDMS allows for the chambers to be filled without reagent loss by pushing the ambient air into the bulk of the elastomer[11]. Chambers are then partitioned by flushing the device with an immiscible fluorinated oil that preferentially wets the channel walls, displacing the remaining aqueous phase and creating an advancing contact line at the PDMS-oil-water interface (**Fig. 1c**). As the contact line moves past the entrance of each access channel, it becomes pinned at the leading edge, causing the aqueous phase at the chamber inlet to thin and ultimately separate from the bulk reagent[12,13]. The array is partitioned in ~1 min. This method allows for the uniform and defect-free partitioning of molecules in an array of 1,000,000 chambers with densities exceeding valve-based digital PCR by a factor of 100 (**Supplementary Notes 1** and **2** and **Supplementary Figs. 2** and **3**).

Although the gas permeability of the device material is needed for dead-end loading, this property also leads to water vapor transport and rapid evaporation during thermocycling, a problem that is exacerbated in reactors with high surface-to-volume ratio (S/V; ~4 × 10^5 m^{-1}). To resolve these competing requirements, we developed a fabrication process to embed a ~2-μm-thick layer of low-permeability polymer (parylene C layer) ~150 μm above the digital PCR array (**Fig. 1b** and **Supplementary Fig. 1**). This layer creates an effective permeation barrier that seals the top of the array, thereby restricting vapor transport to a thin slab of PDMS that becomes saturated after the evaporation of only a small fraction of the reaction volumes (**Supplementary Note 3**). Water vapor gradients at the periphery of the array are controlled by the inclusion of hydration lines (100 μm × 100 μm), which fix the vapor pressure around each 100,000 chamber subarray. The combination of no-flux boundary conditions at the glass and membrane surface, along with the constant vapor pressure enforced by the hydration channels, enables robust single-DNA-molecule amplification and unambiguous detection in picoliter-volume reactors (**Fig. 1d**,**e**).

[1]Centre for High-Throughput Biology, University of British Columbia, Vancouver, British Columbia, Canada. [2]Department of Physics and Astronomy, University of British Columbia, Vancouver, British Columbia, Canada. [3]Department of Chemical and Biological Engineering, University of British Columbia, Vancouver, British Columbia, Canada. [4]Michael Smith Laboratories, University of British Columbia, Vancouver, British Columbia, Canada. [5]Department of Electrical and Computer Engineering, University of British Columbia, Vancouver, British Columbia, Canada. [6]Present address: Biophysics Program, Stanford University, Stanford, California, USA. Correspondence should be addressed to C.L.H. (chansen@phas.ubc.ca).

RECEIVED 24 JANUARY; ACCEPTED 26 MAY; PUBLISHED ONLINE 3 JULY 2011; DOI:10.1038/NMETH.1640

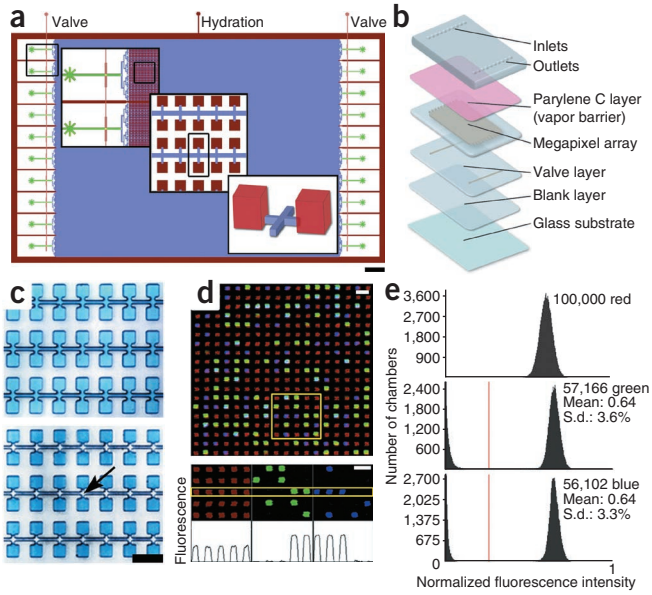

Figure 1 | Megapixel digital PCR using planar emulsion arrays. (**a**) Schematic of megapixel digital PCR device, with insets showing the array and chamber geometries. Hydration channels surrounding the array are shown in red. Scale bar, 3 mm. (**b**) Schematic of the layered device structure, showing the position of the embedded parylene C layer. (**c**) Optical micrograph of reaction chambers filled with blue dye (top) and after oil partitioning (arrow). Scale bar, 50 µm. (**d**) Expanded view of a section of the device showing 342 chambers. The detection of *HLCS* and *RPPH1* sequences from human genomic DNA is visible in green and blue, respectively. Separate fluorescence channels (middle) are shown from boxed region at the top. Intensity profile across the highlighted strip of five chambers is shown at the bottom. Scale bars, 50 µm. (**e**) Histograms of normalized fluorescence intensities over 100,000 chambers. The total number of positive counts as well as the normalized mean and s.d. of fluorescence intensity (arbitrary units) are listed. The red line indicates the threshold used to classify 'positive' and 'negative' chambers.

A digital PCR array of 10^6 chambers provides a theoretical dynamic range of 7 logs (**Supplementary Note 4** and **Supplementary Fig. 4**). To experimentally establish the response of the megapixel device, we measured the abundance of a single-copy gene (*RPPH1* on chromosome 14) over a tenfold serial dilution of human genomic DNA spanning six orders of magnitude in concentrations from 3×10^{-6} haploid genomes to ~2.4 haploid genomes per 10-pl chamber (~920 fg μl^{-1} to ~780 ng μl^{-1}). The observed fraction of chambers showing increased fluorescence through PCR amplification (positive chambers) ranged from 0.00028% to 90.8% and showed excellent agreement with the theoretical binomial response ($R^2 = 0.9978$) (**Supplementary Note 5** and **Fig. 2a**). This is to our knowledge the first demonstration of robust single-molecule detection at total DNA concentration in excess of 30 ng μl^{-1}. By comparison, tube-based qPCR using the same reaction conditions showed both reaction inhibition at high template concentrations and nonspecific background signal in dilute samples, resulting in an effective dynamic range of approximately 10^4 (**Supplementary Fig. 5**). Although difficulties in concentrating genomic DNA beyond 1 µg μl^{-1} precluded measurement of this template at higher concentrations, we performed experiments using a synthetic fragment of the *RPPH1* gene over concentrations ranging from approximately 6×10^{-6} copies per chamber (1 aM) to 9.5 copies per chamber (1.6 pM). These were again in excellent agreement with the theoretical response ($R^2 = 0.9999$) (**Fig. 2a**). At the highest concentrations tested (**Fig. 2a**) we observed a fill factor of 99.994% before reaching saturation, corresponding to an average of 9.7 molecules per chamber.

Next we tested the sensitivity of the megapixel device in detecting rare mutations, defined as the lowest measurable ratio of two target sequences differing by a single-nucleotide variation (SNV ratio). Two-color digital PCR measurements of mixtures of plasmids containing genes encoding wild-type JAK2 kinase and the V617F variant[14] were accurate over relative dilutions ranging from 1:1 to 1:10,000 ($R^2 = 0.9993$) (**Fig. 2b**). We note that the lowest relative concentration measured (10^{-4}) is comparable to the inherent error rate of Taq polymerase, and represents a fundamental limit for methods that use a preamplification step. However, polymerase errors in digital PCR without preamplification should result in the detection of both alleles. Thus we hypothesized that SNV detection at concentrations below the polymerase error rate would be possible by excluding double-positive chambers. To test this, we first loaded a single plasmid into 10^6 chambers at a concentration of 1.39 copies per chamber (~75% positive wells) and detected a total of 38 SNV false positives with detection of both probes in 36 of these chambers (94%), an observation that cannot be explained by random co-localization ($P = 0.001$; binomial test). We did not detect errors that occurred after the first two rounds of amplification (**Supplementary Note 6** and **Supplementary Figs. 6** and **7**); assuming an equal frequency of single-base substitutions, we estimated the polymerase error rate to be between 2.6×10^{-5} and 1.6×10^{-4} per base, which is in close agreement with previously reported values (~3×10^{-5} – 1.1×10^{-4} per base)[7,15]. We next loaded two 500,000-chamber subarrays at relative allele concentrations of one or two in 100,000 alleles (concentration of ~1 plasmid per chamber), and detected a total of 5 and 11 isolated SNV-positive chambers. From this we determined the measured SNV ratio to be 2.7×10^{-5} and 5.9×10^{-5}, respectively (**Supplementary Note 7**). This corresponds to a SNV detection limit of ~ 1:100,000 and is a 5,000-fold increase in sensitivity over off-chip qPCR measurements using an optimized genotyping assay[14] (**Supplementary Fig. 8**).

An array of 1,000,000 chambers has the theoretical precision needed to discriminate a difference in relative concentration of 0.6% with 99% sensitivity and 99% specificity (**Supplementary Note 8** and **Supplementary Fig. 9**). Ten replicate measurements of normal human genomic DNA for two single-copy genes, *RPPH1* and *HLCS* (the latter on chromosome 21), yielded mean copy numbers of 425,885 (s.d. = 652.6; $n = 10$) and 409,435 (s.d. = 639.9) respectively, with an average ratio of *HLCS*/*RPPH1* of 1.040 (s.d. = 0.0027) (**Fig. 2c**). This precision is comparable to the theoretical limit as determined by sampling noise. Independent measurements of the same sample on different devices indicated a significant overrepresentation of the *HLCS* sequence (4.0%, $P = 0.038$; homoscedastic *t*-test). This bias was reduced to 1.5% when measured on a separate sample of genomic DNA, showing that the variation is a property of the template; the source of this sample-specific imbalance is not clear but may be due to differences in DNA fragmentation state or the distribution of single- and double-stranded template. We next evaluated the precision of our device in detecting small allelic imbalances by measuring the relative copy number of the *HLCS* and *RPPH1* genes in normal human genomic DNA spiked with varying amounts of trisomy 21 (T21) genomic DNA ranging from 6% to 2% (**Fig. 2d**). We observed reproducible,

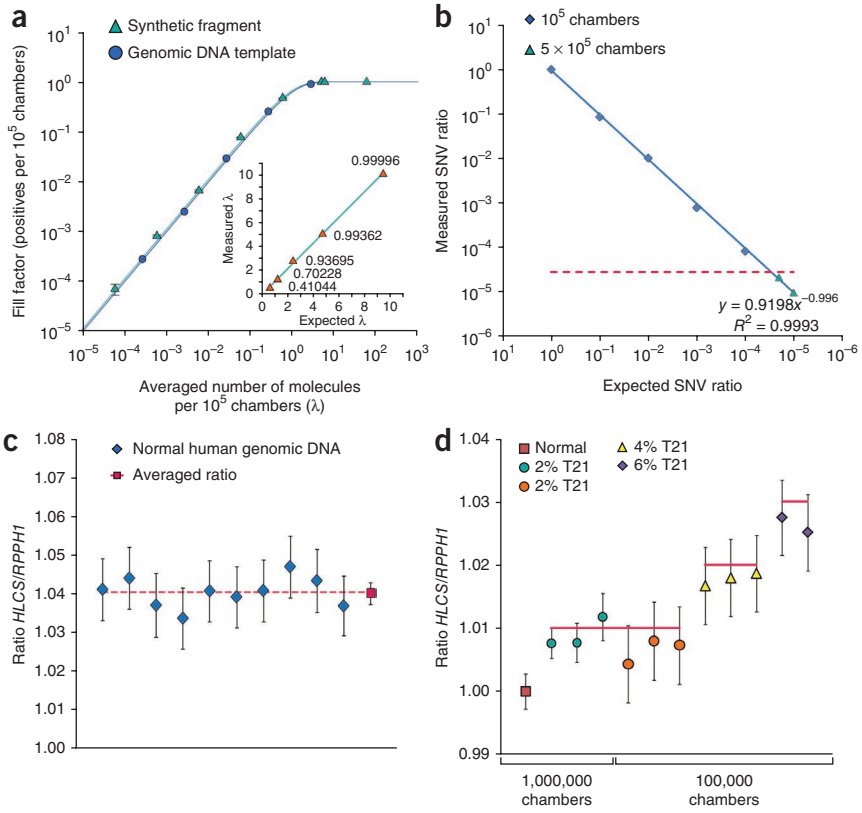

Figure 2 | Dynamic range, sensitivity and precision of megapixel digital PCR. (**a**) Digital PCR response for the *RPPH1* gene measured from dilutions of DNA template and synthetic fragment of *RPPH1* gene. Solid lines show fit to expected binomial distribution for synthetic fragment (R^2 = 0.9999) and genomic DNA (R^2 = 0.9978). Inset, the measured λ values for the synthetic fragment of *RPPH1* (molecules per chamber) at high fill factors (values indicated in the graph) plotted against expected values as determined by dilutions of the stock solution. Solid line shows linear regression ($y = 1.08x$, R^2 = 0.9992). (**b**) Digital PCR measurements of serial dilutions of two plasmids containing either the wild-type sequence or sequence encoding V617F JAK2 at relative dilutions ranging from 1:1 to 1:100,000. Measurements were on subarrays of 10^5 chambers or 5×10^5 chambers. Rate of false positive SNV detection owing to polymerase errors is indicated by dashed line. (**c**) Replicate measurements of the abundance of the *RPPH1* and *HLCS* genes from a single sample of normal human genomic DNA (100,000 chambers) are plotted in the order of relative position across the array. Error bars represent theoretical noise calculated by propagating the binomial noise of each allele (one s.d.) through the ratio. (**d**) Ratios of the *RPPH1* and *HLCS* gene for samples of normal human genomic DNA spiked with 2%, 4% or 6% T21 genomic DNA. All ratios are normalized by that obtained from a matched unspiked sample. Expected values are indicated (red lines). Error bars, theoretical precision defined as 1 s.d. of binomial noise in *HLCS* and *RPPH1* measurements propagated through the ratio.

reliable discrimination of 2% and 3% enrichment using subarrays of 100,000 chambers, whereas 1% enrichment was only well-resolved using full 1,000,000-chamber arrays (**Supplementary Table 1**).

In addition to enabling new measurements in biomedical research and diagnostics, the dramatic increase in assay density in our device has important implications for the adoption of digital PCR as a routine analytical tool. The 1,000,000 chambers may be subdivided into groups of 10,000 chambers, enabling absolute and precise digital PCR analysis on 100 samples per run at a cost and throughput comparable to that of real-time PCR. This approach may be scaled to achieve tens of millions of reactions per device using the same footprint (**Supplementary Note 9**). Thus, we contend that megapixel digital PCR or similar high-density formats will ultimately replace real-time qPCR as the standard analytical tool for DNA measurement.

METHODS

Methods and any associated references are available in the online version of the paper at http://www.nature.com/naturemethods/.

Note: Supplementary information is available on the Nature Methods website.

ACKNOWLEDGMENTS

This research was funded by the Canadian Institute for Health Research (Catalyst NHG-91401), Terry Fox Foundation and the Natural Science and Engineering Research Council. Salary support was provided by the Michael Smith Foundation for Health Research (A.S. and C.L.H.), Natural Science and Engineering Research Council Collaborative Research and Training Experience Genome Science and Technology graduate program (M.V.), the Department of Foreign Affairs and International Trade of Canada (K.A.H.) and the Canadian Institute for Health Research Young Investigator program (C.L.H.). Infrastructure support was provided by Genome British Columbia, Genome Canada and Western Economic Diversification Fund.

AUTHOR CONTRIBUTIONS

K.A.H., C.T., M.V., C.D., A.S., K.L. and C.L.H. developed and optimized the device design. K.A.H. and C.D. developed fabrication protocols and fabricated devices. K.A.H., C.T. and C.D. performed the on-chip digital PCR experiments. K.A.H., O.I.P. and C.B.H. performed the off-chip qPCR experiments. M.V. and C.D. developed image analysis software. K.A.H., C.T., M.V. and C.D. performed data analysis. C.L.H. designed research. K.A.H., C.T., M.V. and C.L.H. wrote the manuscript.

COMPETING FINANCIAL INTERESTS

The authors declare competing financial interests: details accompany the full-text HTML version of the paper at http://www.nature.com/naturemethods/.

Published online at http://www.nature.com/naturemethods/.
Reprints and permissions information is available online at http://www.nature.com/reprints/index.html.

1. Diehl, F. *et al. Nat. Med.* **14**, 985–990 (2008).
2. Warren, L., Bryder, D., Weissman, I.L. & Quake, S.R. *Proc. Natl. Acad. Sci. USA* **103**, 17807–17812 (2006).
3. Fan, H.C. *et al. Proc. Natl. Acad. Sci. USA* **105**, 16266–16271 (2008).
4. Vogelstein, B. & Kinzler, K.W. *Proc. Natl. Acad. Sci. USA* **96**, 9236–9241 (1999).
5. Diehl, F. *et al. Nat. Methods* **3**, 551–559 (2006).
6. Kiss, M.M. *et al. Anal. Chem.* **80**, 8975–8981 (2008).
7. Li, M. *et al. Nat. Methods* **3**, 95–97 (2006).
8. Shen, F. *et al. Lab. Chip* **10**, 2666–2672 (2010).
9. Sundberg, S.O., Wittwer, C.T., Gao, C. & Gale, B.K. *Anal. Chem.* **82**, 1546–1550 (2010).
10. Thorsen, T., Maerkl, S.J. & Quake, S.R. *Science* **298**, 580–584 (2002).
11. Hansen, C.L., Skordalakes, E., Berger, J.M. & Quake, S.R. *Proc. Natl. Acad. Sci. USA* **99**, 16531–16536 (2002).
12. Cohen, D.E., Schneider, T., Wang, M. & Chiu, D.T. *Anal. Chem.* **82**, 5707–5717 (2010).
13. Jackman, R.J. *et al. Anal. Chem.* **70**, 2280–2287 (1998).
14. Bousquet, M. *et al. Hum. Pathol.* **37**, 1458–1464 (2006).
15. Tindall, K.R. & Kunkel, T.A. *Biochemistry* **27**, 6008–6013 (1988).

ONLINE METHODS

Microfluidic device fabrication. All devices were fabricated using the multilayer soft lithography process with modifications to allow for the inclusion of an embedded parylene C layer (**Supplementary Fig. 1a**). The megapixel chip was designed using Clewin (Phoenix Software). Molds were fabricated in a Class 1,000 clean room by contact photolithography on a MA6 mask aligner (SUSS MicroTec) to create multilayer patterns of SU8-2010 (Microchem) and SPR (220-7, Rohm & Haas) photoresist on a 4-inch silicon wafer (Silicon Quest). High-resolution chromium masks for each layer were obtained from Photo Sciences. Immediately before processing the wafers were dried by baking at 190 °C for 10 min to promote resist adhesion. Photoresist exposure and development was performed according to manufacturer specifications. First, a 10-µm-thick layer of SPR-220, spun at 1,400 r.p.m. for 40 s, was used to create channel sections at the entrance and exit of the array where valve actuation is required. After exposure and development, wafers were baked on a hot plate at 115 °C for 20 min to reflow the resist and then hard baked at 190 °C for 60 min to protect this layer during subsequent processing. Next, SU8-2010 photoresist (Microchem), spun to a thickness of 10 µm (3,000 r.p.m. for 30 s), was used to define the feed channels and access channels. Finally, after exposure and development of the first SU8-2010 layer, a second 25-µm-thick (±1 µm) layer of SU8-2010 (820 r.p.m. for 30 s) was used to define the reaction-chamber volumes. Control layer molds, containing valve structures at the entrance and exit of the array, were fabricated on 4-inch wafers using a 25-µm-thick layer of SU8-2025 (Microchem).

To facilitate the release of polymerized PDMS, all molds were coated with a ~200 nm thick layer of poly(paraxylylene) (parylene C) using a Labcoater2 vapor deposition system (Specialty Coatings Systems).

Microfluidic devices were fabricated from molds in a Class 10,000 clean room using consecutive steps of replica molding, vapor deposition and bonding to create multilayer PDMS structures with an embedded parylene C layer and bonded to a glass substrate (**Supplementary Fig. 1b**). The flow layer was fabricated by spinning 5:1 (part A:part B) PDMS (General Electric RTV 615) at 350 r.p.m. for 70 s. After this step, a 2-µm-thick layer of parylene C was deposited directly onto the unpolymerized PDMS. During this process, the parylene di-radical monomers polymerize directly over the PDMS that contains free unsaturated carbon-carbon bonds. Molds were then cured for 15 min at 80 °C, vulcanizing the PDMS and resulting in an optically smooth parylene C layer. To activate the surface of the parylene C layer, the molds were then oxidized for 20 s with O_2 plasma at 600 mTorr (Harrick Plasma cleaner, high power). The activated parylene C layer was next functionalized by spin-coating (1,000 r.p.m. for 30 s) a solution containing 10% (v/v) tetra(ethylorthosilicate) (Sigma), 4% (v/v) 3-methacryloxypropyltri(methoxy)-silane (Sigma), 0.2% (v/v) allyltri(methoxy)silane (Sigma) and 10% (v/v) 0.2 N HCl in ethanol. After curing at 90 °C for 15 min in a vacuum oven (with vacuum), 54 g of degassed 5:1 PDMS (General Electric RTV 615) was poured on top of the silanized parylene layer and cured for 1 h at 80 °C. The silanization treatment resulted in a strong bond between the functionalized parylene C layer and the PDMS. (**Supplementary Fig. 1a–d**). The hybrid PDMS-parylene-PDMS chip was then peeled off the flow mold, and inlet and outlet ports were punched using a 20 gauge coring tool (Technical Innovations). The flow layer was then aligned in a push-up geometry (**Supplementary Fig. 1b**) to the PDMS coated control layer (20:1 General Electric RTV 615, spun at 1,750 r.p.m. for 30 s and baked at 80 °C for 60 min). The aligned layers were bonded by baking at 80 °C for 60 min to create a monolithic multilayer device. The device was then bonded to a blank PDMS layer prespun on a glass slide (GE, 20:1 RTV A:B, spun at 1,750 rpm for 30 s and baked at 80 °C for 30 min) by baking at 190 °C in a vacuum oven for 1 h (starting at 80 °C). Finally, the entire microfluidic device was coated with an additional layer of parylene C (~2 µm) to enclose it with a hermetic vapor barrier. All the devices were kept in airtight containers (99.5% humidity) for at least 48 h before use.

Device operation. All reaction components, including PCR master mix, probes, primers and template, were assembled and mixed off chip before analysis in microfluidic digital PCR arrays. Preassembled PCRs were dead-end loaded into the device at 12 pounds per square inch (p.s.i.) with the exit port of the array blocked by the actuation of integrated microvalves (25 p.s.i.). After complete filling, FC40 oil (3M) was injected into the main flow channel at 14 pounds per square inch (p.s.i.), displacing the PCR mix from the feed channels. The total analysis time was ~5 h: PCR preparation took ~1 h; reagent loading and chamber filling, ~15 min; partitioning, ~1 min; thermocycling, ~1 h; scanning, ~2 h; and image analysis, ~15 min.

To avoid dehydration effects at the array periphery, hydration channels surrounding the array were loaded with hydration fluid containing 1× ABI Fast PCR Mastermix (Life Technologies), 5% glycerol (Invitrogen), 0.5 mg ml^{-1} dextran (Fluka, MW ~6,000 g mol^{-1}). Hydration lines were kept pressurized at 14 p.s.i. during thermocycling. The hydration fluid contained 500 nM free Quasar670 fluorophore (Biosearch Technologies), which served as a fluorescent marker for image analysis.

PCR conditions. All on-chip digital PCRs were performed using ABI Fast PCR Mastermix and were supplemented with 1× DA sample loading reagent (Fluidigm) and 500 nM of free Quasar670 fluorophore to serve as a passive reference dye. To minimize pipetting variability, all components were premixed before dispensing aliquots in different tubes and adding template solutions.

Microfluidic devices were thermocycled on a flatbed thermocycler block (Bio-Rad DNA Engine PTC-200; MJ Research) with light mineral oil (Fisher Scientific) added between the thermocycler block and the glass slide to ensure good thermal contact over the entire array. The thermocycling protocol for the human genomic DNA included a 20 s hot start at 90 °C and 40 cycles of two-step PCR (93 °C for 1 s and 61 °C for 30 s). Thermocycling protocols for the JAK2 experiments consisted of a 20 s hot start at 90 °C and 40 cycles at 93 °C for 1 s and 58 °C for 30 s.

Human genomic DNA template was obtained from BioChain (D1234-152) and prepared at specified concentrations in TE buffer pH 7.5. Human T21 genomic DNA was obtained from American Type Culture Collection (CCL-54D). All genomic DNA samples were heated for 15 min at 95 °C before analysis. Concentrations and dilutions were verified with a NanoDrop spectrometer (Thermo Scientific) (R^2 = 0.998 between tenfold dilutions) until reaching the detection limit of the instrument (~0.1 ng $µl^{-1}$). For dynamic-range measurements, a synthetic

doi:10.1038/nmeth.1640

double-stranded fragment identical to the sequence targeted on the human genomic DNA for *RPPH1* was synthesized by Integrated DNA Technologies. Both complimentary single-stranded sequences (**Supplementary Table 2**) were synthesized and pooled together at a concentration of 10 μM, denatured at 95 °C for 10 min and cooled down to 4 °C before dilution into TE buffer pH 7.5. After dilution, all stock solutions were kept frozen at −20 °C. Plasmids carrying the wild-type and the mutant JAK2 genes were provided by C. Haynes (Chemical and Biological Engineering, University of British Columbia) and were diluted from concentrated stocks into TE buffer at pH 7.5.

Primer and probe sequences and concentrations used in digital PCR analysis of *RPPH1* (ribonuclease P RNA component H1, *HLCS* (holocarboxylase synthetase (biotin-(proprionyl-CoA-carboxylase (ATP-hydrolyzing)) ligase) and *JAK2* SNVs are listed in **Supplementary Table 2**. Spectrally distinct allele specific fluorescence hydrolysis minor groove–binding (MGB) probes for the wild-type JAK2 sequence (VIC-labeled) and the V617F SNV (FAM-labeled) were obtained from Life Technologies (primer and probe sequences are provided in **Supplementary Table 2**). Hydrolysis probes for *RPPH1* (FAM) and *HLCS* (CalOrange560) were obtained from Biosearch Technologies. Off-chip qPCR experiments were performed on a Bio-Rad DNA Engine mounted with a Chromo4 detector in 20-μl PCR volumes. Genomic DNA analysis was performed using a 95 °C hot start step and the same cycling protocols as for on-chip experiments. Amplification curves were generated by the Opticon Monitor 3 software and were normalized using the same Quasar670 passive dye as used in digital PCR experiments. Off-chip *JAK2* SNV qPCR analysis was performed using optimized protocols developed for diagnostic testing. Reactions were assembled using ABI genotyping mix with 300 nM primers and 200 nM of the two MGB probes. Thermocycling was performed using a 2 min heating step at 50 °C, 10 min hot start at 95 °C, followed by 40 cycles of 95 °C for 15 s and 60 °C for 60 s. Amplification curves were generated by Opticon Monitor 3 software. Expected cycle threshold (Ct) values were calculated based on the measured Ct at a SNV ratio of 1:1 and (100% mutant to wild type ratio) and assuming PCR efficiency of 100%.

Image analysis. After PCR, the microfluidic device was imaged using a microarray scanner (Wellscope, Biomedical Photometrics) with optics for simultaneous imaging three spectrally distinct fluorescent probes (FAM, CalO 560 and Quasar670; Biosearch Technologies). The resulting images were stored in BigTiff format with measured fluorophore intensities stored in separate color channels (RGB) at 0.5 pixels μm^{-1}. Custom image analysis software written in C was used for automated segmentation of chambers (using the passive dye) and counting of positive chambers. Chamber segmentation was performed using manual specification of three control points chosen in the top left (x_L,y_T), top right (x_R,y_T) and bottom left (x_L,y_B) corners of the subarray to be analyzed. From the control points the algorithm defines basis vectors for the array:

$$\vec{v}_x = \frac{(x_R, y_T) - (x_L, y_T)}{|(x_R, y_T) - (x_L, y_T)|}\delta, \qquad \vec{v}_y = \frac{(x_L, y_B) - (x_L, y_T)}{|(x_L, y_B) - (x_L, y_T)|}\delta$$

where δ refers to the pitch of the array. Starting at the stop left control point the segmentation algorithm sequentially found each chamber by stepping one basis vector to the approximate position of the next chamber center and then finding the chamber center by locally minimizing the following 'electrostatic potential' function computed on a 40 pixel by 40 pixel neighborhood centered at expected chamber location computed as:

$$V(x,y) = \sum_{i=-20}^{20} \sum_{j=-20}^{20} -p(x+i, y+j)/(i^2 + j^2),$$

where $p(x,y)$ is the passive dye value located at pixel x,y. The algorithm then updated the new starting position and repeated this process, reading each row of the array from left to right, until all chambers were located. If a chamber was found 15 or more pixels away from its expected location or if $-9{,}000 < V(x,y)$ at the center of the chamber, the chamber segmentation was marked as defective and not included in the analysis. Intensity measurements for each of the three-color channels at each chamber were then computed by summing the pixel intensities over a 20 pixel by 20 pixel square centered at each chamber. The intensities for probe fluorophores (green and blue) were normalized to the passive fluorophore (red). A histogram of the chamber intensities was then constructed, and a threshold was automatically determined by maximizing the difference between class variances of positive and negative chambers.